Bergmann, P., Kashubin, A., Ivandic, M., Lueth, S., Juhlin, C. (2014): Time-lapse difference static correction using prestack crosscorrelations: 4D seismic image enhancement case from Ketzin. - *Geophysics*, *79*, 6, p. B243-B252

DOI: http://doi.org/10.1190/geo2013-0422.1

GEOPHYSICS, VOL. 79, NO. 6 (NOVEMBER-DECEMBER 2014); P. B243–B252, 10 FIGS.
10.1190/GEO2013-0422.1

## Case History

# Time-lapse difference static correction using prestack crosscorrelations: 4D seismic image enhancement case from Ketzin

Peter Bergmann[1], Artem Kashubin[2], Monika Ivandic[3], Stefan Lüth[1], and Christopher Juhlin[3]

## ABSTRACT

A method for static correction of time-lapse differences in reflection arrival times of time-lapse prestack seismic data is presented. These arrival-time differences are typically caused by changes in the near-surface velocities between the acquisitions and had a detrimental impact on time-lapse seismic imaging. Trace-to-trace time shifts of the data sets from different vintages are determined by crosscorrelations. The time shifts are decomposed in a surface-consistent manner, which yields static corrections that tie the repeat data to the baseline data. Hence, this approach implies that new refraction static corrections for the repeat data sets are unnecessary. The approach is demonstrated on a 4D seismic data set from the Ketzin $CO_2$ pilot storage site, Germany, and is compared with the result of an initial processing that was based on separate refraction static corrections. It is shown that the time-lapse difference static correction approach reduces 4D noise more effectively than separate refraction static corrections and is significantly less labor intensive.

## INTRODUCTION

In the processing of reflection seismic data, statics refer to time shifts that are caused by shallow velocity variations and topographical changes. Most commonly, they are corrected by assigning time corrections to the respective shot and receiver positions in two steps (Dahl-Jensen, 1989): (1) refraction static corrections consisting of a correction for elevation and a correction for variations in refracted wave traveltimes (Lawton, 1989) and (2) residual static corrections to take care of the remaining variations by shifting the traces in the normal moveout corrected CDP gathers, e.g., by maximizing the stack power (Ronen and Claerbout, 1985).

Time-lapse seismic measurements also face these aspects in a vintage-dependent sense because changes in statics due to changes in the near-surface conditions are known to be first-order contributors to time-lapse noise (Kragh and Christie, 2002; Cantillo, 2011). Considerable changes in the statics of repeated onshore seismic surveys can occur due to precipitation-related changes in soil moisture and in the groundwater table. Offshore surveys can be affected by variable tidal statics or changes in water salinity and temperature. Production-related or injection-related processes can cause considerable velocity changes (Hatchell and Bourne, 2005; Fuck et al., 2011; Haugvaldstad et al., 2011), which leave time-shift imprints on time-lapse seismic data that can be very similar to those of near-surface velocity variations. In this context, accurate static correction is an essential prerequisite for quantitative time-lapse interpretation methods that are based on time shifts (Landrø and Stammeijer, 2004; Rickett et al., 2007; Trani et al., 2011; Chadwick et al., 2012; White, 2013).

In processing of time-lapse seismic data, refraction and residual static corrections may be used to account for the above phenomena and enhance the stack coherency of the individual data set vintages, yet they often fail to yield optimal difference images because even minor relative time shifts between the stacks can cause considerable spurious time-lapse energy.

At the onshore Ketzin site, we found that refraction static corrections followed by residual static corrections gave poor results on repeated 2D and 3D seismic surveys (Bergmann et al., 2011; Lüth

Manuscript received by the Editor 13 November 2013; revised manuscript received 18 March 2014; published online 9 October 2014.
[1]GFZ German Research Centre for Geosciences, Helmholtz Centre Potsdam, Centre for Geological Storage, Potsdam, Germany. E-mail: bergmann@gfz-potsdam.de; slueth@gfz-potsdam.de.
[2]WesternGeco, Schlumberger House, Buckingham Gate, West Sussex, UK. E-mail: akashubin@slb.com.
[3]Uppsala University, Department of Earth Sciences, Uppsala, Sweden. E-mail: monika.ivandic@geo.uu.se; christopher.juhlin@geo.uu.se.

et al., 2011; Ivanova et al., 2012). The main reason for this is the general inability of refraction static corrections to provide sufficiently accurate velocity models of the weathered layer, which is due to three factors. First, the inherent band limitation of seismic data and an often nonoptimum signal-to-noise ratio (S/N) make a reliable first-break determination in many cases impossible. Second, the solution to refraction static problems can be nonunique (Palmer, 2010a, 2010b). Third, when a time-lapse project continues over a longer period, first-break picking and inversion are likely to be carried out by different processors. Hence, a variable degree of experience and individual subjectivity can add further nonrepeatability.

In this work, we propose to solve the problem through a more data-driven approach that is not limited to the removal of time shifts within the individual time-lapse surveys. Rather, we seek to accommodate for static differences between them. This is achieved by means of a static correction in which the relative time shifts between the baseline and repeat trace pairs are derived automatically, decomposed in a surface-consistent manner, and applied to the repeat data to tie them to the baseline data.

The paper is structured as follows. First, we establish the proposed time-lapse difference static correction method. Subsequently, we introduce the 4D data set from the Ketzin site, which will be used for illustration of the method. To evaluate our results, we will use the results reported by Ivandic et al. (2012) and Ivanova et al. (2012) as reference. We then continue with the estimation of the statics differences from the 4D data, their decomposition, and the resulting static corrections. Finally, we present the enhanced 4D difference volumes that were obtained by this static correction approach and interpret the statics solution in light of precipitation-related velocity changes in the near surface.

## TIME-LAPSE DIFFERENCE STATIC CORRECTION METHODOLOGY

The application of surface-consistent models for the reduction of time shifts in CDP gathers makes use of the concepts proposed by Taner et al. (1974), Taner and Koehler (1981), and Ronen and Claerbout (1985). We extend this model to time-lapse seismic measurements and consider, therefore, a baseline survey as the standard. The statics associated with the baseline data are $S_i^{\text{base}}$ for sources and $R_j^{\text{base}}$ for receivers. Subsequently, a repeat survey is conducted that differs from the baseline survey by changes in the near-surface velocities, resulting in the statics, $S_i^{\text{rep}}$ and $R_j^{\text{rep}}$. In comparison to its corresponding baseline trace, each repeat trace will have a lag $D_{ij}$ that is composed of the source static difference $\Delta S_i = S_i^{\text{rep}} - S_i^{\text{base}}$ and receiver static difference $\Delta R_j = R_j^{\text{rep}} - R_j^{\text{base}}$. This leads to the following surface-consistent model:

$$D_{i,j} = \Delta S_i + \Delta R_j + \Delta C_{p(i,j)} + n_{i,j}. \tag{1}$$

The term $\Delta C_{p(i,j)}$ accounts for the statics differences that are associated with the CDP, with $p(i, j)$ denoting the CDP index that is assigned to source $i$ and receiver $j$. Thereby, $\Delta C_{p(i,j)}$ is representing those time shifts that may be due to stress-induced velocity changes or compaction/dilation of the reservoir. Furthermore, $n_{ij}$ denotes the residuals in statics differences that cannot be explained through this model. To solve equation 1 iteratively for the individual components of the statics differences, we adopt an error-weighted Gauss-Seidel procedure (e.g., Yilmaz, 2001):

$$\begin{aligned}
S_i^{(k)} &= \left(\sum_{[j]\in \mathrm{CSG}_i}^{N_i^s} \omega_{ij}\right)^{-1} \times \left(\sum_{[j]\in \mathrm{CSG}_i}^{N_i^s} \omega_{ij}(D_{ij} - S_i^{(k-1)} - R_j^{(k-1)} - C_{p(i,j)}^{(k-1)})\right)\\
R_j^{(k)} &= \left(\sum_{[i]\in \mathrm{CRG}_j}^{N_j^r} \omega_{ij}\right)^{-1} \times \left(\sum_{[i]\in \mathrm{CRG}_j}^{N_j^r} \omega_{ij}(D_{ij} - S_i^{(k-1)} - R_j^{(k-1)} - C_{p(i,j)}^{(k-1)})\right)\\
C_p^{(k)} &= \left(\sum_{[i,j]\in \mathrm{CDP}_p}^{N_p^c} \omega_{ij}\right)^{-1} \times \left(\sum_{[i,j]\in \mathrm{CDP}_p}^{N_p^c} \omega_{ij}(D_{ij} - S_i^{(k-1)} - R_j^{(k-1)} - C_p^{(k-1)})\right)
\end{aligned} \tag{2}$$

where $k$ denotes the iteration index. The term $[j] \in \mathrm{CSG}_i$ denotes the set of receivers that belongs to the common-shot gather (CSG) of source $j$. The term $[i] \in \mathrm{CRG}_i$ denotes the set of sources that belong to the common-receiver gather (CRG) of receiver $i$. Accordingly, $[i, j] \in \mathrm{CDP}_p$ denotes the source-receiver pairs that are associated with the $p$th CDP. $N_i^s$ is the number of traces in the $i$th CSG, $N_i^r$ is the number of traces in the $j$th CRG, and $N_p^c$ is the fold of the $p$th CDP. Furthermore, the error weights $w_{ij}$ are used to account for the S/N in the trace pairs. The weights are defined by the correlation coefficients of the initial (uncorrected) trace pairs $r_{ij}^{in}$ and the correlation coefficients of the trace pairs after correction to optimum lag $r_{ij}^{\text{opt}}$ as follows:

$$\omega_{ij} = \begin{cases} 0 & \text{for } r_{ij}^{\text{opt}} \le r_{ij}^{in} \\ \log_{10}(r_{ij}^{\text{opt}} - r_{ij}^{in}) & \text{for } r_{ij}^{\text{opt}} > r_{ij}^{in} \end{cases}. \tag{3}$$

The size of a weight determines the significance of the respective time shift in the decomposition. If the coherency of a trace pair improves considerably when shifted to optimum lag ($r_{ij}^{\text{opt}} \gg r_{ij}^{in}$), it is given a relatively large weight. If $r_{ij}^{\text{opt}} \le r_{ij}^{in}$, the trace pair is either already at optimum lag or one of the traces might be dead. In either case, the respective static difference value is ignored throughout the decomposition. The logarithm of the correlation coefficient differences is used to compress and flatten their distributions.

To address long wavelength components in the decomposition, a moving-average smoothing is performed after each iteration. The smoother gives a regularization-type control on spatial contrasts in the decomposed solution. For each station, the average static solution of all stations that are located within a given search radius is assigned to a smoothed solution, which is subsequently blended back into the unsmoothed solution.

The decomposition starts with null vectors $S_i^{(0)}$, $R_j^{(0)}$, and $C_p^{(0)}$ as initial values. After each iteration, the solution of the current $S_i^{(k)}$, $R_j^{(k)}$, and $C_p^{(k)}$ is added to those of the previous iterations to be used as $S_i^{(k-1)}$, $R_j^{(k-1)}$, and $C_p^{(k-1)}$ in the next iteration. This procedure is iteratively continued until convergence, which can be determined by monitoring the root mean square (rms) of $n_{ij}$. When the decomposition terminates, the cumulated solutions are retrieved as final estimates of the static differences $\Delta S_i$, $\Delta R_j$, and $\Delta C_p$ (equation 1).

Throughout this paper, we will refer to this approach as time-lapse difference (TLD) static correction. In the time-lapse processing workflow, one can implement the TLD static correction after the baseline refraction and residual static corrections (Figure 1). It is also conceivable to calculate and apply the new residual static corrections for the repeat survey after the TLD statics. However, this

would lead to an improvement in stack power of the repeat data at the cost of the tie to the baseline data. In either case, it is important to note that the TLD static correction requires calculation of refraction statics only once because the same baseline refraction statics are also applied to the repeat data sets, thus avoiding picking first breaks on the repeat data sets.

## KETZIN 4D SEISMIC DATA SET

The first experimental onshore geologic $CO_2$ storage site in Europe was established in Ketzin, located approximately 25-km west of Berlin, Germany, in 2004. The objective of the pilot-scale research project was to provide practical experience in the operation and monitoring of a geologic $CO_2$ storage site (Schilling et al., 2009; Würdemann et al., 2010; Martens et al., 2011, 2012, 2013). Injection of $CO_2$ started in June 2008 under the $CO_2$SINK project and has continued in the framework of the $CO_2$MAN project since 2010. The site is situated in the eastern part of the Roskow-Ketzin double anticline where a brine-bearing reservoir (Triassic sandstones of the Stuttgart Formation) is present at a depth of approximately 630–650 m (Figure 2a). The $CO_2$ is injected in well $CO_2$ Ktzi 201/2007, which will be abbreviated to Ktzi201 in this paper. Two additional observation wells, $CO_2$ Ktzi 200/2007 and $CO_2$ Ktzi 202/2007, were drilled in 2007, and a third observation well $CO_2$ Ktzi 203/2012 was drilled in September 2012. The sandstones of the Stuttgart Formation consist of sandy channel facies rocks with good reservoir properties alternating with muddy floodplain facies rocks of poor reservoir quality (Förster et al., 2006; Norden et al., 2010). The upper seal of the Stuttgart Formation is the Weser Formation, which consists mainly of mudstones and anhydrite (Beutler et al., 1999) with a total thickness of approximately 80 m (Norden et al., 2010). The top of the Weser Formation contains a 10–20-m-thick anhydrite layer, known as the Heldburg-Gips or K2 horizon, which constitutes a prominent seismic reflector in this area (Juhlin et al., 2007). The K2 is overlain by mudstones and carbonates of the Arnstadt Formation that exhibit similar sealing properties to those of the Weser Formation. In the shallower sandstones of the lower Jurassic, natural gas was stored at depths of 250–400 m. Due to economic reasons, this gas storage was abandoned in 2000. The seal to the former gas storage, the muddy sediments of the Pliensbachian group, provides a second barrier to the deeper $CO_2$ storage. A third barrier is constituted by the Tertiary Rupelian clays, which are present with a thickness of approximately 80 m. The near-surface layers are mainly composed of Quaternary sands and tills that exhibit a relatively flat surface topography.

An important component within the Ketzin project is the geophysical monitoring of the $CO_2$ migration in the subsurface.

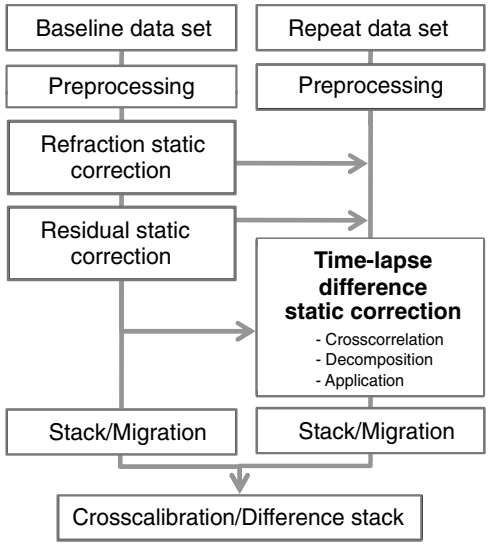


Figure 1. Implementation of the TLD static correction in a generic time-lapse seismic processing workflow.

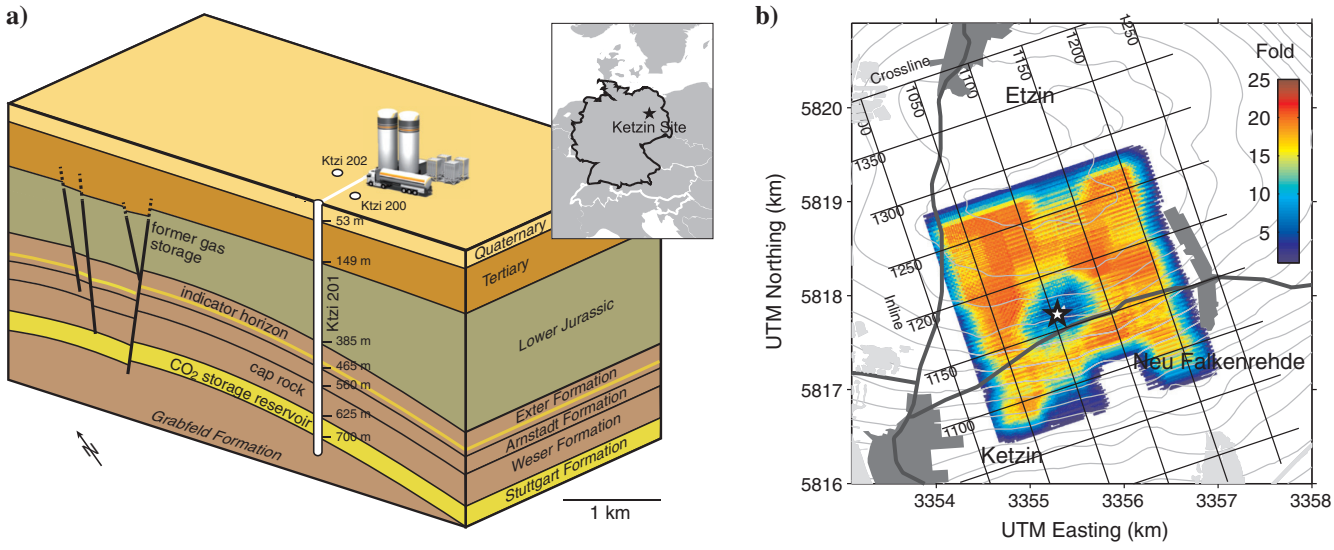


Figure 2. (a) Schematic of the anticline geology at the Ketzin site (after Liebscher et al., 2012) and its location in Germany (inset). The injection well $CO_2$ Ktzi 201/2007 is marked as Ktzi201. The two further observation wells drilled in 2007 are marked as Ktzi200 and Ktzi202. (b) Survey area and fold of the first repeat 3D seismic acquisition (acquired in 2009) with the system of inlines and crosslines. The location of the injection well Ktzi201 is marked by a star. Gray contours are isodepth lines to the near top reservoir (Stuttgart Formation). The anticline top is approximately 1.5-km north of the injection site.

Therefore, a broad range of seismic methods was performed, including 3D surveys (Juhlin et al., 2007; Ivanova et al., 2012), sparse 3D surveys (Ivandic et al., 2012), 2D surveys (Bergmann et al., 2011), crosswell surveys, and moving source profilings (Yang et al., 2010, Götz, 2013). We will focus on the repeated 3D seismic surveys.

The baseline 3D survey was acquired in 2005 and covered an area of approximately 14 km$^2$ (Juhlin et al., 2007). This survey aimed not only as a baseline for subsequent repeat surveys, but also provided a detailed characterization of the site. It showed the east–west-trending faults on the crest of the Ketzin anticline, a clear signature from the remnant natural gas storage in the lower Jurassic Formations and gave indications of sandy reservoir channels within the heterogeneous Stuttgart Formation.

In 2009, after an injection of approximately 22 kilotons of $CO_2$, a first repeat survey was performed covering a 7-km$^2$ subset of the baseline area (Figure 2b). This repeat survey provided the most comprehensive view of the $CO_2$ migration to date by imaging changes in the reflectivity at the reservoir level (Figure 3). This reflectivity change has an extent of approximately 250 m in the north–south direction and approximately 350 m in the east–west direction with a tendency of higher seismic amplitudes toward the west (Lüth et al., 2011). Based on this, Ivanova et al. (2012) performed a volumetric estimation by an interpretation of the amplitude change at the reservoir top and the reflection pull-down below the reservoir. Although reporting a reasonable match between the estimate and the amount of $CO_2$ actually injected, they also found time-lapse noise to be present throughout the difference volume. This finally led to an update of the imaging workflow and a reprocessing of the baseline static corrections (Ivanova et al., 2012).

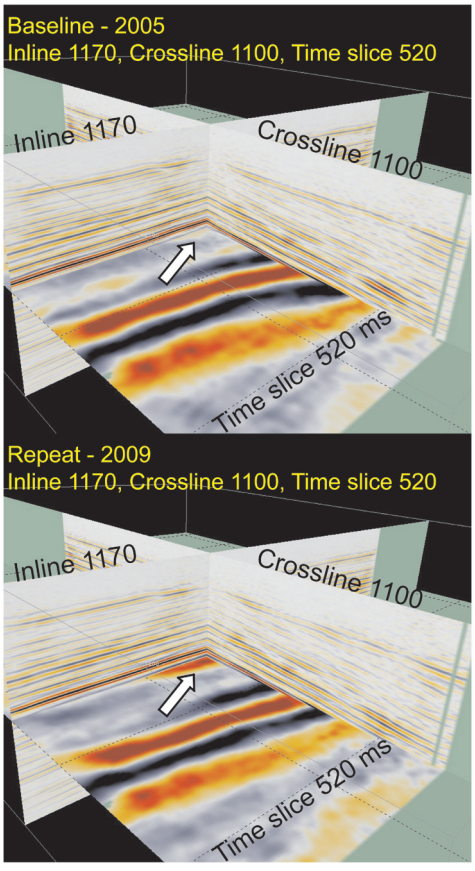


Figure 3. Cross sections through the baseline and repeat seismic volumes. The amplitude anomaly at the intersection of inline 1170 and crossline 1100 (approximate location of injection well Ktzi201) at approximately 520 ms indicates the presence of the injected $CO_2$.

Regarding this matter, Kashubin et al. (2011) show that differences in the first-break times between the baseline and the first repeat survey were most likely due to velocity changes in the near surface. They also found that the first-break times correlate with cumulative precipitation at the location prior to data acquisition, which, in turn, has an impact on the near-surface velocities. We will therefore address the findings of Kashubin et al. (2011) again in the final section of this paper.

The work presented here builds on experience gained from testing different static correction methods on the repeated 2D seismic surveys at the Ketzin site (Bergmann et al., 2011). It was found that a surface-consistent approach, similar to that described above, was particularly useful to reduce static differences. Hence, we present an extension of this approach to the 4D data from the Ketzin site, which is further introducing a CDP component and data weights in the decomposition.

## ESTIMATION OF TRACE-TO-TRACE STATIC DIFFERENCES

The initial step of the proposed TLD static correction method is estimating the tracewise static differences in the prestack data (i.e., $D_{ij}$ in equation 1). Therefore, we process the time-lapse data sets identically, according to the workflow of Ivanova et al. (2012) up to the stage prior to CDP stacking. To carry out trace-to-trace crosscorrelations, the preprocessed data sets were merged and sorted into pairs of corresponding baseline and repeat traces. The static differences were retrieved from these pairs as the lags for which the crosscorrelations reach maximum. To avoid cycle skips, we constrained the lags to the interval of $\pm 10$ ms (25 ms is the dominant period in the data). Prior to the computation of the crosscorrelations, cosine-tapered top and bottom mutes (taper length 50 ms) have been applied to the traces. The time gates for these mutes were applied as offset-dependent functions and computed for a normal moveout (NMO) velocity of 2000 m/s. In the following, when indicating gate start times and gate end times, we will refer to the time gates at zero-offset two-way time (TWT).

To investigate the choice of an optimum time gate, several time gates were tested for a random subset of the full data sets (Figure 4). In this test, the mean change in correlation coefficients of full traces $\Delta r$ was computed for a range of gate start times and gate end times by

$$\Delta r = \frac{1}{N}\sum_{n=1}^{N} r_n^{\text{opt}} - r_n^{in}. \tag{4}$$

The optimum lag for an entire trace was determined from the crosscorrelation maximum of the data in the selected time gate, but the actual average correlation coefficients were determined for the entire trace. Similar to the data weights used in equation 3, $\Delta r$ was selected for the assessment of the time gates. Hence, large positive $\Delta r$ values indicate that the estimated lags align the baseline

repeat-trace pairs well, whereas negative values indicate that the lags result in an overall alignment reduction that is prone to generate a poorer time-lapse result.

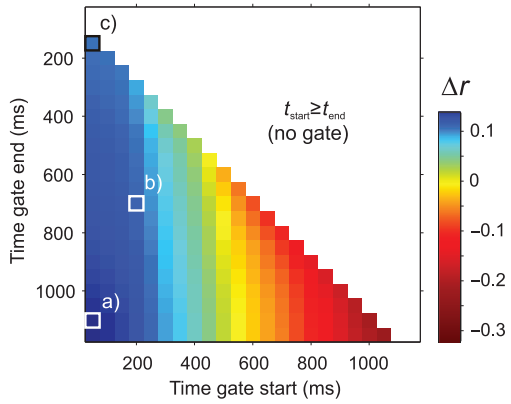


Figure 4. Mean difference of the correlation coefficients $\Delta r$ for variable length and position of the correlation time gate. Time gate starts and time gate ends refer to zero-offset TWT. A positive $\Delta r$ indicates an enhanced trace alignment across the time-lapse data sets and vice versa. The square boxes mark time gates (a) 50–1100 ms, (b) 200–700 ms, and (c) 50–150 ms. Computation of $\Delta r$ values was carried out using a random subset (10,000 trace pairs) of the full 3D data sets.

Figure 4 shows mean changes of the correlation coefficients for various time gates that provides two conclusions: First, short gates at small TWTs produce better alignments than gates of the same length at larger TWTs. This is caused by the fact that the statics are better resolved in the first breaks than by the late portions of the traces. As a result, the time shifts obtained from the late windows generally yield reduced alignments in the trace pairs (lower right corner in Figure 4). Second, long time gates provide better alignments than short time gates (lower left corner in Figure 4).

Based on these findings, we selected three time gates for a more detailed investigation: 50–1100 ms (full trace), 200–700 ms (focus on imaging target), and 50–150 ms (focus on first breaks). We performed the decomposition of the statics obtained within the three gates, applied these statics to the repeat data set, and produced brute stacks. Figure 5 compares the poststack repeatability improvements associated to the three time gates in terms of the normalized rms (NRMS) (Kragh and Christie, 2002).

Although these graphs show that the poststack repeatability can be considerably improved by the TLD static correction, they give no preference for a distinct time gate. Thus, we conclude that, within this selection of traces, the time gates will lead to rather equivalent time-lapse results and opted for the 200–700-ms gate in the remainder of this study (Figure 5c). The influence of the injected $CO_2$ on reflection traveltimes below the reservoir (a push-down effect) appeared to be negligible in our case. This

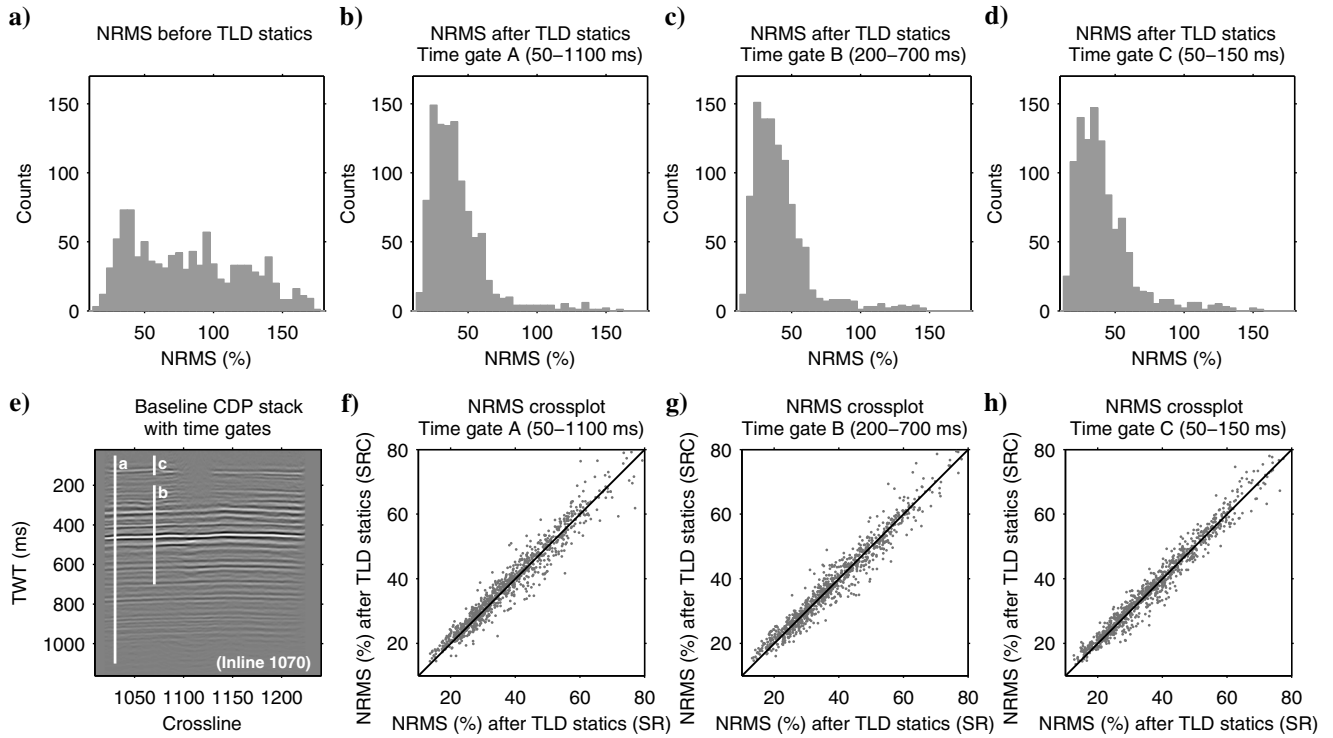


Figure 5. Testing the time gates for estimation of the trace-to-trace static differences. (a) NRMS values of the difference of baseline stack and repeat stack obtained from independent refraction static corrections. (b-d) NRMS values of the same data after time-lapse static corrections based on the tracewise static differences obtained from the three time gates. (e) Inline section of the baseline processing (after Juhlin et al., 2007) intersecting the injection location at crossline 1100. The vertical lines indicate the three time gates. Note that the time gates were applied as offset-dependent mute gates and are displayed here only at zero-offset TWT. Time-gate *C* is mainly focused on the first breaks, which were muted during the CDP stack processing. The injection reservoir is located at approximately 520-ms TWT. (f-g) Crossplots for the time gates showing the NRMS after static correction of the source and receiver components (*x*-axis) against the NRMS after static correction of the source, receiver, and CDP components (*y*-axis).

relatively small amount of gas (approximately 22 kilotons) is enough to produce a noticeable amplitude anomaly, but not enough to substantially affect the traveltimes. However, in the general case in which a 4D signal might comprise significant time-lapse amplitudes and push-down/pull-up of underburden reflections, the time gates should be constrained to overburden reflections.

## DECOMPOSITION OF THE STATIC DIFFERENCES

For the final decomposition parameters, we empirically selected a radius of 300 m for the spatial smoother. We assessed the convergence of the iterative decomposition from the rms value of the residual delays $n_{ij}$, which proved to converge (change <1%) after

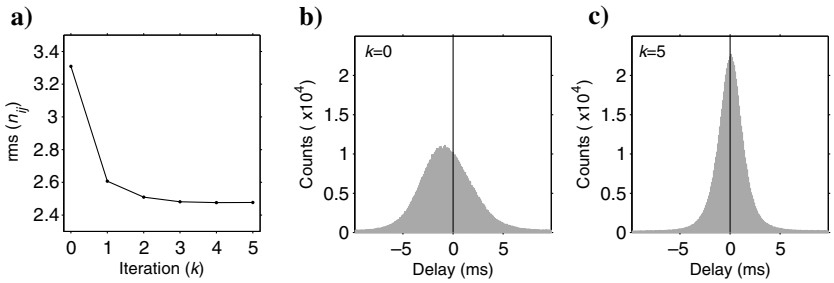


Figure 6. (a) Evolution of the delays during the decomposition. Delay distributions in the prestack data (b) before and (c) after applying the TLD static correction. Note that the negative bias in (b) is removed by the TLD static correction.

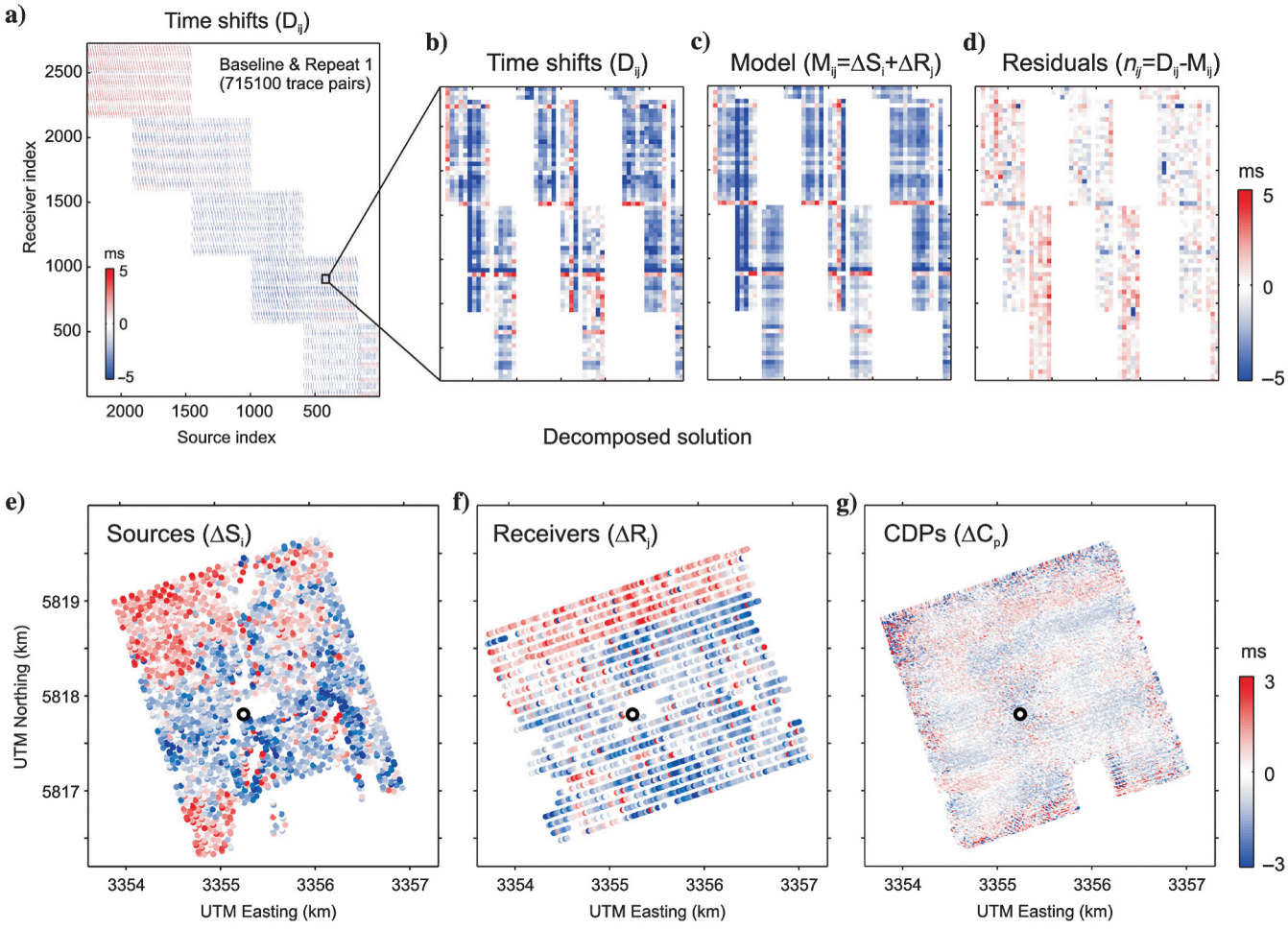


Figure 7. Application of the TLD static correction to the Ketzin 4D data. (a) Trace-to-trace time shifts ($D_{ij}$ in equation 1) estimated from windowed crosscorrelation. (b) Zoomed view of the time shifts. (c) Source and receiver solutions (shown in subfigures e and f) mapped back to the trace data. (d) Difference between the time shifts and the model solution, which equals the remaining delays after TLD static correction. (e-g) Source, receiver, and CDP solutions after surface-consistent decomposition of the delays. The circle indicates the location of the injection site.

4–5 iterations from an initial rms of approximately 3.3 ms to a final one of approximately 2.4 ms (Figure 6a). It is noteworthy that this was effective in removing the initial 0.6-ms bias among the data sets (compare Figure 6b and 6c).

Figure 7 provides a graphical representation of equations 1 and 2 illustrating the decomposition results. Figure 7a shows the map of the crosscorrelation lags in source-receiver index axes, and Figure 7e and 7g shows the decomposed components in geographic coordinates. The source and receiver solutions show negative values in the southern and central part of the area and positive values to the north. Maximum absolute values of the source and receiver solutions reach up to 5.3 ms. In contrast, the CDP component shows a rather random pattern with no imprint around the $CO_2$ injection well (Figure 7g). Although we selected the correlation time gates such that they contain the reservoir, this supports that the decomposed components are mainly associated to velocity changes in the near surface.

## APPLICATION OF THE TIME-LAPSE DIFFERENCE STATIC CORRECTION

To compare the difference stack obtained from the TLD static corrections with that from the individual refraction static corrections (Figure 8), both data sets were processed identically. Replicating the steps of Ivanova et al. (2012), additional poststack crosscalibration was carried out to match the amplitude, frequency, and phase characteristics of the repeat stacks with the baseline stack.

In general, we observe that the repeat stack with TLD static corrections (applied after the baseline refraction and residual statics as of the workflow in Figure 1) contains reflections that are as coherent as the baseline stack (with the original refraction and residual statics, Figure 8a) and the repeat stack with the new refraction (from repicked first breaks) and new residual statics (not shown in this paper). However, the stack difference reveals that the TLD static correction leads to a more favorable 4D S/N in the difference stack. The inline section (Figure 8c) shows that the $CO_2$-induced time-lapse signature stands out more clearly with the TLD static correction applied. In addition, some undesired amplitude differences in the shallow stack portions are significantly reduced.

The crossline section (Figure 8f) shows that the time-lapse noise persists in those areas in which the fold is low (inline range 1060–1120; see also Figure 2). The inline range 1200–1240 displays an amplitude anomaly at 200–300 ms that originates from the abandoned natural gas storage. Previously, it was not obvious whether this anomaly was a processing artifact or due to real physical changes as a consequence of ongoing gas migration or/and pressure changes. Given that the signature is found consistently in both difference stacks (Figure 8e and 8f), migration of the remnant gas is rather likely to be a reason for the anomaly than the processing.

Figure 8g and 8h shows the normalized amplitude difference maps along the reservoir top. Although both images are consistent in the shape of the anomaly, the TLD static stack is providing a more detailed delineation of the signature. For instance, the TLD statics stack difference exhibits less 4D amplitudes toward the south of the injection well.

The NRMS maps of Figure 9 reveal that the S/N improvement introduced by the TLD statics is more significant than that introduced by the poststack crosscalibration. More specifically, the

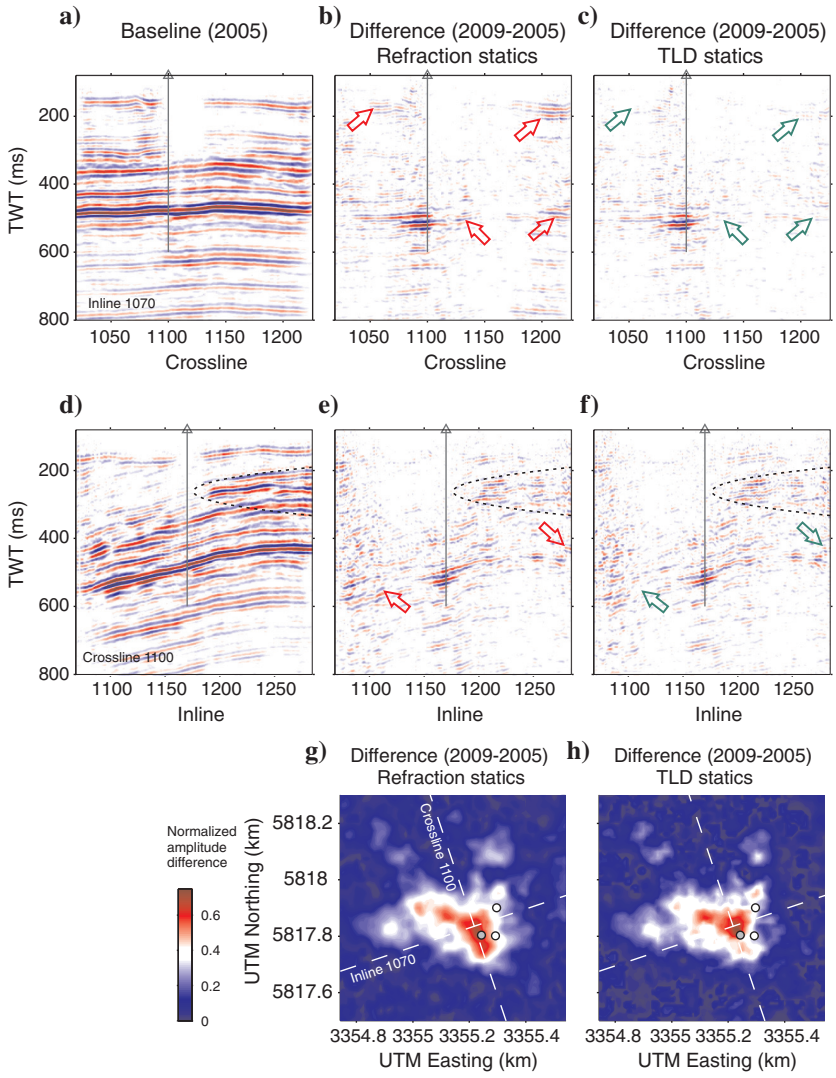


Figure 8. Cross sections through the difference volumes in the vicinity of the injection borehole (indicated by gray vertical line). (a) Inline section of the baseline stack (after Juhlin et al., 2007). (b) The same inline section showing time-lapse amplitude differences obtained with the refraction static corrections (after Ivanova et al., 2012), and (c) with the TLD static corrections. (d) Crossline section of the baseline stack (after Juhlin et al., 2007). The dashed line outlines those stack portions in which the seismic amplitudes are affected by interpreted remnant natural gas. (e) The same inline section showing amplitude differences obtained with refraction static corrections (after Ivanova et al., 2012) and (f) with TLD static corrections. Amplitude difference horizons at the reservoir level (g) obtained with refraction static corrections (after Ivandic et al., 2012) and (h) with TLD static correction. The gray dot indicates the location of the injection well.

TLD static map before the poststack crosscalibration (Figure 9b) reaches almost the NRMS values of the calibrated refraction static map (Figure 9c). This is remarkable because the uncalibrated data have not yet undergone any wavelet matching at this point. This indicates that the uncalibrated TLD statics stack difference is already near an optimal NRMS, which can, in principle, be achieved through time shifting of the prestack data. Additional poststack NRMS improvements are due to residual time shift removal as well as amplitude, frequency, and phase calibrations. Figure 9b and 9d shows that this improved particularly the NRMS in the northern part of the area.

## CORRELATION OF TIME-LAPSE DIFFERENCE STATICS AND PRECIPITATION PATTERNS

The initial motivation for updating the refraction static corrections of the repeat survey by Ivanova et al. (2012) was driven by changes in the near surface due to different weather conditions at the times of the surveys (Kashubin et al., 2011). When the 2009 repeat data set was processed with the original baseline static corrections (from 2005) and compared with the original 2005 seismic volume, a clear northwest–southeast trend in the poststack crosscorrelation time shifts between the volumes was observed (Figure 10a). In the repeat volume, the same horizons appeared to be shallower in the northwestern part of the area, but deeper in the southeastern part. Moreover, many reflections at various depths did not stack up as coherently as in the baseline volume. Repicking the first arrivals and calculating new refraction static corrections accommodated the changes in the near surface to some extent. The poststack crosscalibration minimized further the time-lapse noise. Interestingly, the poststack crosscorrelation time shifts between the volumes (Figure 10a) reveal a pattern similar to that of the surface-related TLD static components (Figure 7e and 7f).

The averaged difference in first arrival times between the baseline and repeated data sets (Figure 10b) shows a very similar trend to that in Figure 10a. This suggests that the main changes occurred in the near surface as the refracted waves represented by the first arrivals sample only a relatively shallow part of the volume. This conclusion is also confirmed by the analysis of the optimal time gates used for the TLD statics algorithm: the short shallow gates and the longer deep gates were found to produce comparable time shifts (Figure 5), and therefore, these time shifts are due to the changes in the shallow subsurface that affect the entire traces.

Kashubin et al. (2011) show that, at the Ketzin site, the first-break differences (and refraction static time shifts to a lesser extent) are strongly dependent on the soil moisture saturation, which, in turn, depends on the cumulative precipitation at the location before and during acquisition of each survey (Figure 10d).

The reprocessed baseline refraction static corrections of Ivanova et al. (2012) differ from the initial baseline refraction corrections by up to ±10 ms for sources and receivers. Figure 10c shows the differences in the tracewise refraction static corrections (receiver static + source static) plotted at the source-receiver midpoint locations. These differences are greater than the averaged differences in the first breaks (Figure 10b). They do not replicate the same northwest–southeast trend as in the first-break differences and in the poststack crosscorrelation time shifts (Figure 10a and 10b, respectively). The different pattern can be explained by the influence of the surface topography (Figure 10e), which is included in the refraction statics model and affects the solution.

The near-surface soil conditions and weathering may well be topography related (e.g., stiffer rocks are less affected by weathering and result in higher elevations; lower topography is likely to yield higher water saturation). As a result, the moisture-related time delays are expected to be different for different parts of the survey area. For the different vintages of the seismic data, time

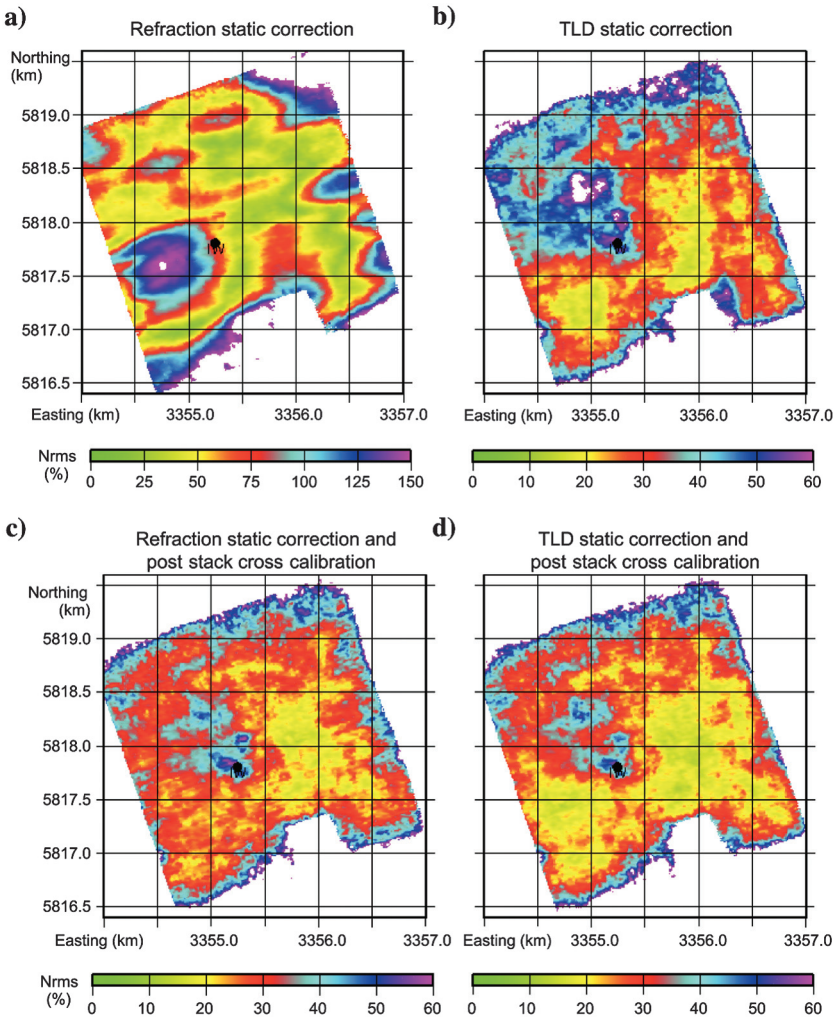


Figure 9. (a and c) Maps of the NRMS errors between the baseline and repeat volumes with refraction static correction and (b and d) TLD static correction. (a and b) show the NRMS errors before poststack crosscalibration and (c and d) after poststack crosscalibration. Note in (a) the different scale and the present long-wavelength patterns that are unresolved by the refraction static corrections. The black dot marks the location of the injection well.

delays (and refraction statics corrections) may depend nonlinearly on a combination of topography and soil water saturation. Therefore, even with the same topography, the solution depends on the input and has the imprint of the first breaks and the starting model, which makes it difficult to assess the resulting differences in the refraction statics pattern and to correlate them with changes in the near surface.

In contrast, the total TLD statics (Figure 10f) show a clear correlation with changes in the near surface, i.e., with the difference in cumulative precipitation in Figure 10d and, consequently, with the TLD in the first arrivals in Figure 10b. Hence, this correlation with precipitation could provide a strategy for estimating spatially varying operators from the rainfall records that may be used in prestack crossequalizations of the time-lapse data sets. Conversely, the solution of the TLD static shifts could be used for an inversion of near-surface velocity changes or soil moisture saturation changes.

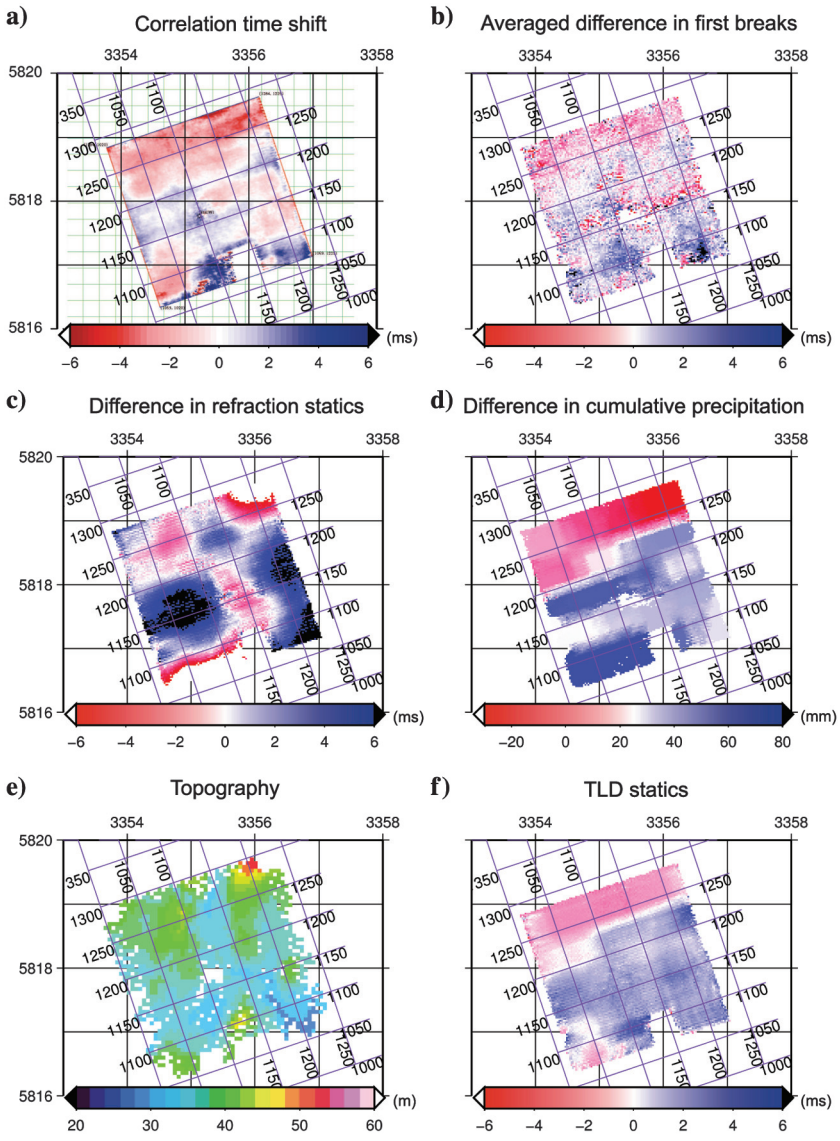


Figure 10. Maps of (a) the correlation time shift between the seismic volumes stacked with the original baseline refraction statics, (b) the TLD in the first arrivals averaged for the source-receiver midpoints, (c) the time-lapse difference in refraction static corrections, (d) the difference in cumulative precipitation, (e) the local topography, and (f) prestack TLD static shifts ($D_{ij} = \Delta S_i + \Delta R_j$; see Figure 7e and 7f). The data are plotted according to the CMP positions.

## CONCLUSIONS

Velocity changes in the near surface are known to have a negative impact on time-lapse seismic images when not accurately compensated by static corrections. Refraction static corrections are, in this respect, of limited use, as they consider only the statics for the individual time-lapse surveys.

As an alternative, we propose a TLD static correction that is focused on the accommodation of static changes between the time-lapse data sets. This TLD static correction estimates the static differences from crosscorrelations and decomposes them in a surface-consistent manner. Therefore, it does not require first-break picking and inversion for velocities from repeat data sets. In this respect, the TLD static correction can be considered as a type of residual static correction that can automatically be extended to the processing of future repeat data sets.

We tested the TLD static correction for a 4D case study from the Ketzin $CO_2$ storage site, Germany. As a reference, we used the results that were obtained from a recent processing in which refraction static corrections were performed individually on the time-lapse data sets. Even though the TLD static correction method is considerably less time-consuming, we found that it provides a stack difference with an enhanced S/N.

This Ketzin case study shows that the pattern of the TLD statics is highly consistent with patterns in the cumulative precipitation data. This observation confirms that near-surface velocity changes are due to changes in the soil moisture saturation and that an efficient compensation for them can be achieved by the TLD static corrections.

## ACKNOWLEDGMENTS

The authors thank all partners of the $CO_2$SINK and $CO_2$MAN (www.co2ketzin.de) projects for their support. The research described in this paper is funded by the European Commission (Sixth and Seventh Framework Program), the German Federal Ministry of Economics and Technology, and the German Federal Ministry of Education and Research and industry. Further funding from the Federal Ministry of Education and Research within the GEOTECHNOLOGIEN Program (this paper has the number GEOTECH-2092) and industry partners enabled this research. The $CO_2$MAN project acknowledges its industry partners: VNG, Vattenfall, RWE, Statoil, Dillinger Hüttenwerke, Saarstahl, and OMV.

We are grateful to P. Smith, E. Kragh, P. Christie, J. Wood, and A. Dawson of Schlumberger and WesternGeco for critical comments on the

manuscript. We further thank three anonymous reviewers for improving the quality of the manuscript.

## REFERENCES


Bergmann, P., C. Yang, S. Lüth, C. Juhlin, and C. Cosma, 2011, Timelapse processing of 2D seismic profiles with testing of static correction methods at the $CO_2$ injection site Ketzin (Germany): Journal of Applied Geophysics, **75**, 124–139, doi: 10.1016/j.jappgeo.2011.05.005.

Beutler, G., N. Hauschke, and E. Nitsch, 1999, Faziesentwicklung des Keupers im Germanischen Becken, *in* N. Hauschke, and V. Wilde, eds., Trias, eine ganz andere Welt: Verlag.

Cantillo, J., 2011, A quantitative discussion on time-lapse repeatability and its metrics: 81st Annual International Meeting, SEG, Expanded Abstracts, 4160–4164.

Chadwick, R. A., G. A. Williams, J. D. O. Williams, and D. J. Noy, 2012, Measuring pressure performance of a large saline aquifer during industrial-scale $CO_2$ injection: The Utsira Sand, Norwegian North Sea: International Journal of Greenhouse Gas Control, **10**, 374–388, doi: 10.1016/j.ijggc.2012.06.022.

Dahl-Jensen, T., 1989, Static corrections on crystalline rock: Geophysical Prospecting, **37**, 467–478, doi: 10.1111/j.1365-2478.1989.tb02218.x.

Förster, A., B. Norden, K. Zinck-Jørgensen, P. Frykman, J. Kulenkampff, E. Spangenberg, J. Erzinger, M. Zimmer, J. Kopp, G. Borm, C. Juhlin, C. Cosma, and S. Hurter, 2006, Baseline characterization of the $CO_2$SINK geological storage site at Ketzin, Germany: Environmental Geosciences, **13**, 145–161, doi: 10.1306/eg.02080605016.

Fuck, R. F., I. Tsvankin, and A. Bakulin, 2011, Influence of background heterogeneity on traveltime shifts for compacting reservoirs: Geophysical Prospecting, **59**, 78–89, doi: 10.1111/j.1365-2478.2010.00909.x.

Götz, J., 2013, Borehole seismic monitoring of $CO_2$ storage within a saline aquifer at Ketzin, Germany: Ph.D. thesis, Technical University Berlin.

Hatchell, P., and S. Bourne, 2005, Rocks under strain: Strain-induced time-lapse time shifts are observed for depleting reservoirs: The Leading Edge, **24**, 1222–1225, doi: 10.1190/1.2149624.

Haugvaldstad, H., B. Lyngnes, P. Smith, and A. Thompson, 2011, Ekofisk time-lapse seismic — A continuous process of improvement: First Break, **29**, 113–120.

Ivandic, M., C. Yang, S. Lüth, C. Cosma, and C. Juhlin, 2012, Time-lapse analysis of sparse 3D seismic data from the $CO_2$ storage pilot site at Ketzin, Germany: Journal of Applied Geophysics, **84**, 14–28, doi: 10.1016/j.jappgeo.2012.05.010.

Ivanova, A., A. Kashubin, N. Juhojuntti, J. Kummerow, J. Henninges, C. Juhlin, S. Lüth, and M. Ivandic, 2012, Monitoring and volumetric estimation of injected $CO_2$ using 4D seismic, petrophysical data, core measurements and well logging: A case study at Ketzin, Germany: Geophysical Prospecting, **60**, 957–973, doi: 10.1111/j.1365-2478.2012.01045.x.

Juhlin, C., R. Giese, K. Zinck-Jørgensen, C. Cosma, H. Kazemeini, N. Juhojuntti, S. Lüth, B. Norden, and A. Förster, 2007, 3D baseline seismics at Ketzin, Germany: The $CO_2$SINK project: Geophysics, **72**, no. 5, B121–B132, doi: 10.1190/1.2754667.

Kashubin, A., C. Juhlin, A. Malehmir, S. Lüth, A. Ivanova, and N. Juhojuntti, 2011, A footprint of rainfall on land seismic data repeatability at the $CO_2$ storage pilot site, Ketzin, Germany: 81st Annual International Meeting, SEG, Expanded Abstracts, 4165–4169.

Kragh, E., and P. Christie, 2002, Seismic repeatability, normalized RMS and predictability: The Leading Edge, **21**, 640–647, doi: 10.1190/1.1497316.

Landrø, M., and J. Stammeijer, 2004, Quantitative estimation of compaction and velocity changes using 4D impedance and traveltime changes: Geophysics, **69**, 949–957, doi: 10.1190/1.1778238.

Lawton, D. C., 1989, Computation of refraction static corrections using first-break traveltime differences: Geophysics, **54**, 1289–1296, doi: 10.1190/1.1442588.

Liebscher, A., S. Martens, F. Möller, and M. Kühn, 2012, On-shore $CO_2$ storage in Germany — Experiences gained from the Ketzin pilot site, Brandenburg, the sole German national $CO_2$ storage project, *in* J. Gluyas, and S. Mathias, eds., Geoscience of carbon dioxide ($CO^2$ storage): Woodhead Publishing Limited.

Lüth, S., P. Bergmann, C. Cosma, N. Enescu, R. Giese, J. Gotz, A. Ivanova, C. Juhlin, A. Kashubin, C. Yang, and F. Zhang, 2011, Time-lapse seismic surface and down-hole measurements for monitoring $CO_2$ storage in the $CO_2$SINK project (Ketzin, Germany): Energy Procedia, **4**, 3435–3442, doi: 10.1016/j.egypro.2011.02.268.

Martens, S., T. Kempka, A. Liebscher, S. Lüth, F. Möller, A. Myrttinen, B. Norden, C. Schmidt-Hattenberger, M. Zimmer, and M. Kühn, 2012, Europe's longest-operating on-shore $CO_2$ storage site at Ketzin, Germany: A progress report after three years of injection: Environmental Earth Sciences, **67**, 323–334, doi: 10.1007/s12665-012-1672-5.

Martens, S., A. Liebscher, F. Möller, J. Henninges, T. Kempka, S. Lüth, B. Norden, B. Prevedel, A. Szizybalski, M. Zimmer, and M. Kühn, , and the Ketzin Group, 2013, $CO_2$ storage at the Ketzin pilot site, Germany: Fourth year of injection, monitoring, modelling and verification: Energy Procedia, **37**, 6434–6443, doi: 10.1016/j.egypro.2013.06.573.

Martens, S., A. Liebscher, F. Möller, H. Würdemann, F. Schilling, and M. Kühn, 2011, Progress report on the first European on-shore $CO_2$ storage site at Ketzin (Germany) — Second year of injection: Energy Procedia, **4**, 3246–3253, doi: 10.1016/j.egypro.2011.02.243.

Norden, B., A. Förster, D. Vu-Hoang, F. Marcelis, N. Springer, and I. Le Nir, 2010, Lithological and petrophysical core-log interpretation in $CO_2$SINK, The European onshore research storage and verification project: SPE Reservoir Evaluation and Engineering, **13**, 179–192, doi: 10.2118/115247-PA.

Palmer, D., 2010a, Non-uniqueness with refraction inversion — A syncline model study: Geophysical Prospecting, **58**, 203–218, doi: 10.1111/j.1365-2478.2009.00818.x.

Palmer, D., 2010b, Non-uniqueness with refraction inversion — The Mt Bulga shear zone: Geophysical Prospecting, **58**, 561–575, doi: 10.1111/j.1365-2478.2009.00855.x.

Rickett, J., L. Duranti, T. Hudson, B. Regel, and N. Hodgson, 2007, 4D time strain and the seismic signature of geomechanical compaction at genesis: The Leading Edge, **26**, 644–647, doi: 10.1190/1.2737103.

Ronen, J., and J. Claerbout, 1985, Surface-consistent residual statics estimation by stack-power maximization: Geophysics, **50**, 2759–2767, doi: 10.1190/1.1441896.

Schilling, F., G. Borm, H. Würdemann, F. Möller, and M. Kühn, 2009, Status report on the first European on-shore $CO_2$ storage site at Ketzin (Germany): Energy Procedia, **1**, 2029–2035, doi: 10.1016/j.egypro.2009.01.264.

Taner, M., F. Koehler, and K. Alhilali, 1974, Estimation and correction of near-surface time anomalies: Geophysics, **39**, 441–463, doi: 10.1190/1.1440441.

Taner, M. T., and F. Koehler, 1981, Surface consistent corrections: Geophysics, **46**, 17–22, doi: 10.1190/1.1441133.

Trani, M., R. Arts, O. Leeuwenburgh, and J. Brouwer, 2011, Estimation of changes in saturation and pressure from 4D seismic and AVO time-shift analysis: Geophysics, **76**, no. 2, C1–C17, doi: 10.1190/1.3549756.

White, D. J., 2013, Toward quantitative $CO_2$ storage estimates from time-lapse 3D seismic travel times: An example from the IEA GHG Weyburn–Midale $CO_2$ monitoring and storage project: International Journal of Greenhouse Gas Control, **16**, S95–S102, doi: 10.1016/j.ijggc.2013.01.047.

Würdemann, H., F. Möller, M. Kühn, G. Borm, and F. Schilling, , $CO_2$SINK-Group, 2010, The field-laboratory for $CO_2$ storage "$CO_2$SINK" at Ketzin (Germany): Site preparation, baseline surveys, and the first year of operation: International Journal of Greenhouse Gas Control, **4**, 938–951, doi: 10.1016/j.ijggc.2010.08.010.

Yang, C., C. Juhlin, N. Enescu, C. Cosma, and S. Lüth, 2010, Moving source profile data processing, modelling and comparison with 3D surface seismic data at the $CO_2$SINK project site, Ketzin, Germany: Near Surface Geophysics, **8**, 601–610, doi: 10.3997/1873-0604.2010022.

Yilmaz, Ö., 2001, Seismic data analysis: SEG.